



ISSN: (Print) (Online) Journal homepage: <https://www.tandfonline.com/loi/gcoo20>


# Preparation of nano-TiO<sub>2</sub> sensitized by new ruthenium complex for photocatalytic degradation of methylene blue under visible light irradiation

Shabnam Alizadeh & Reza Takjoo

To cite this article: Shabnam Alizadeh & Reza Takjoo (2022): Preparation of nano-TiO<sub>2</sub> sensitized by new ruthenium complex for photocatalytic degradation of methylene blue under visible light irradiation, Journal of Coordination Chemistry, DOI: [10.1080/00958972.2022.2070743](https://doi.org/10.1080/00958972.2022.2070743)

To link to this article: <https://doi.org/10.1080/00958972.2022.2070743>

 View supplementary material [↗](#)

 Published online: 09 May 2022.

 Submit your article to this journal [↗](#)

 Article views: 21

 View related articles [↗](#)

 View Crossmark data [↗](#)



# Preparation of nano-TiO<sub>2</sub> sensitized by new ruthenium complex for photocatalytic degradation of methylene blue under visible light irradiation

Shabnam Alizadeh and Reza Takjoo

Department of Chemistry, Faculty of Science, Ferdowsi University of Mashhad, Mashhad, Iran

## ABSTRACT

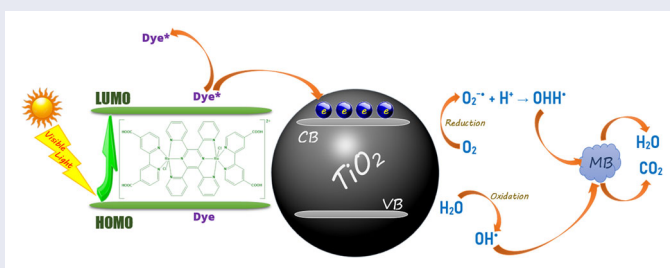
In this work we have synthesized *cis/trans*-[Cl(L)Ru(*tppz*)Ru(L)Cl](ClO<sub>4</sub>)<sub>2</sub> (L = 2,2'-bipyridine-4,4'-dicarboxylic acid, *tppz* = tetra-2-pyridinylpyrazine) with the main objective to apply it in photocatalytic reactions. The TiO<sub>2</sub> is sensitized with the complex to apply visible light more effectively in the photocatalytic reactions. The structure and optical properties of the photocatalyst were characterized by FT-IR, XRD, TEM, FE-SEM, EDX, DRS, BET and UV-vis spectroscopy. The FT-IR and EDX analysis confirmed the chemisorption of the ruthenium complex on the nano-TiO<sub>2</sub> surface. According to the XRD, TEM and FE-SEM analysis it is concluded that the existence of ruthenium complex is not affected by the crystal structure and morphology of nano-TiO<sub>2</sub>. However, BET showed an increase in the surface area after dye-sensitization. The characterization results revealed that the dye-sensitized TiO<sub>2</sub> has a wider absorption spectrum range than nano-TiO<sub>2</sub>. To evaluate the photocatalytic activity of the product, the photo degradation of the methylene blue was studied. The synthesized product could degrade 87% methylene blue in simulating waste water.


## ARTICLE HISTORY


Received 8 June 2021  
Accepted 18 April 2022

## KEYWORDS

Nano-TiO<sub>2</sub>; photocatalytic; methylene blue; visible light; dye-sensitized



**CONTACT** Reza Takjoo  [r.takjoo@um.ac.ir](mailto:r.takjoo@um.ac.ir), [rezatakjoo@yahoo.com](mailto:rezatakjoo@yahoo.com)  Department of Chemistry, Faculty of Science, Ferdowsi University of Mashhad, Mashhad, Iran

 Supplemental data for this article is available online at <https://doi.org/10.1080/00958972.2022.2070743>.

© 2022 Informa UK Limited, trading as Taylor & Francis Group

## 1. Introduction

In recent years, due to the phenomena of industrialization there is an increase in chemical pollutants such as dyes, sulfates and toxic compounds in earth and water resources. This is a great threat to human health and a pervasive problem [1–3]. Researchers are investigating to find ways to reduce environmental pollution. One of the most ideal ways, that is currently being considered, is the use of heterogeneous photocatalysis in solar energy [4]. Among photocatalysts,  $\text{TiO}_2$  due to its interesting properties such as non-toxicity, physical and chemical stability, high redox potential, low cost and ease of use, is the most common photocatalyst [5–7]. However, the large band gap of  $\text{TiO}_2$  (3.2 eV) limits its performance in the visible region; therefore, in the case of photocatalytic applications it can only be used within the ultraviolet region. Unfortunately, the UV region is a very small fraction of the sunlight (3.0–5.0%) [8]. To overcome this issue, many methods have been applied such as physical methods [9], metals doped [10] and dye-sensitization [11, 12] to modify nano-sized  $\text{TiO}_2$  to be used in the visible region. Among these different strategies, sensitization has been more prominent in recent years. There are two advantages for the  $\text{TiO}_2$ -photosensitization systems, the photosensitizer is able to transfer electrons to conduction band of  $\text{TiO}_2$  through absorption of visible light, as well as control the charge separation and recombination dynamics at the sensitizer/nanocrystal interfaces [13].

Ruthenium(II) polypyridyl complexes of 2,2'-bipyridine (*bpy*), 1,10-phenanthroline (*phen*), and related ligands are widely used in the dye-sensitized solar cells (DSSC) [14–16]. The importance of the dyes is due to the carboxylic acid groups that can anchor to the hydroxyl-bearing surfaces [17]. Therefore, the ruthenium bipyridyl complex  $[\text{Ru}(4,4'\text{-H}_2\text{dcby})_2(\text{SCN})_2]$  ( $\text{N}_3$  dye), which contains the carboxylic group, is one of the most successful, widely studied sensitizers [18].

In the last few decades, synthesis of binuclear metal complexes with a suitable bridge ligand that leads to the formation of stable mixed valence states attracts attention [19–22]. These compounds are important in biological processes [23], molecular electronics [24], and also theoretical studies of electron transfer kinetics [25]. The presence of the pyrazine ligand in the Creutz–Taube complex as a powerful bridge arose interests of researchers to design binuclear ruthenium(II) complexes with pyrazine ligands such as 2,3-bis(2-pyridyl)aminoxaline [26], 2,2'-bipyrimidine [27–30] and 2,3-bis(2-pyridyl)pyrazine [31, 32]. Homo- or hetero-polynuclear ruthenium complexes are well synthesized with *tppz* and  $\pi$ -acidic (e.g. 2,2'-bipyridine, 2,2',6',2''-terpyridine) and  $\sigma$ -donor (monodentate amines) are most used as the terminal ligands [33]. The UV-vis spectrum of all these compounds shows there is an acceptable absorption in the visible region. This absorption is related to the Ru  $[d(\pi)]\text{-}tppz(\pi^*)$  MLCT transition. This encouraged us to design and synthesize a complex containing *tppz* and a terminal bipyridine ligand with a carboxylic substituent that can attach to the nano- $\text{TiO}_2$  surface and provide a dye-sensitized photocatalyst.

In this paper, *cis/trans*- $[\text{Cl}(\text{L})\text{Ru}(tppz)\text{Ru}(\text{L})\text{Cl}](\text{ClO}_4)_2$  (structure shown in Figure 1) is synthesized as the dye to attached to the  $\text{TiO}_2$  surface. Moreover, the photocatalytic degradation of the methylene blue (MB) in the presence of visible light irradiation in aqueous media is investigated with the prepared photocatalyst.

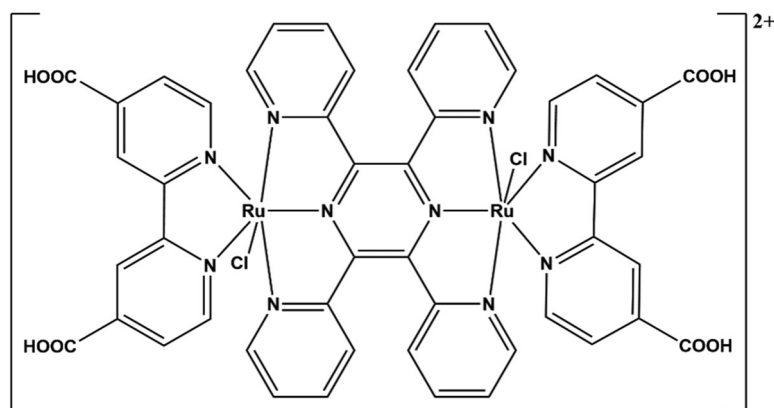


**Figure 1.** Structure of *cis/trans*-[Cl(L)Ru(*tppz*)Ru(L)Cl](ClO<sub>4</sub>)<sub>2</sub>.

## 2. Experimental

### 2.1. Materials

The commercial TiO<sub>2</sub> P25 powder containing 80% anatase and 20% rutile was bought from Iranian Nanomaterials Pioneers. The starting ruthenium precursor [Cl<sub>3</sub>Ru<sup>III</sup>(μ-*tppz*)Ru<sup>III</sup>Cl<sub>3</sub>] was prepared by following literature procedures [34]. RuCl<sub>3</sub>·8H<sub>2</sub>O, tetra(2-pyridyl)pyrazine (*tppz*), 2,2'-bipyridine-4,4'-dicarboxylic acid (*H<sub>2</sub>dcbpy*) and other commercially available chemicals and solvents were used as received from Merck Chemicals and Sigma-Aldrich Chemicals.

### 2.2. Synthesis

The precursor complex [Cl<sub>3</sub>Ru(μ-*tppz*)RuCl<sub>3</sub>] (80 mg, 0.1 mmol), free ligand (*H<sub>2</sub>dcbpy*) (46 mg, 0.25 mmol), LiCl (42 mg, 2 mmol) and NEt<sub>3</sub> (0.4 cm<sup>3</sup>) were taken in DMF (20 cm<sup>3</sup>) and refluxed for 6 h under a nitrogen atmosphere. The light green solution gradually converted to deep green. By reducing pressure, solvent was evaporated. Saturated aqueous NaClO<sub>4</sub> solution was then added to the solution and the precipitated solid filtered and washed by cold ethanol and then ice cold water.

### 2.3. Photocatalyst preparation

TiO<sub>2</sub> nanoparticles sensitized by *cis/trans*-[Cl(L)Ru(*tppz*)Ru(L)Cl](ClO<sub>4</sub>)<sub>2</sub> were prepared as following: 1 g of TiO<sub>2</sub> and 0.005 g of the ruthenium complex were added into 50 mL of DMF. Then the mixture was refluxed for 12 h. The solid was washed with DMF until the filtrate was colorless and dried for 8 h at 60 °C in an oven.

### 2.4. Measurement of photocatalytic activity

The photocatalytic activity was surveyed through degradation of MB as model pollutant under visible light irradiation. A 150 W OSRAM Powerstar HQI-TS lamp with a cut-off λ < 400 nm was used as the light source. Catalyst (3 mg) was added to 50 mL MB

aqueous solution (50 mg/L) in a 100-mL Dewar reactor. In order to achieve adsorption equilibrium between the catalyst surface and the organic molecules, the solution was stirred in the dark for 30 min. The sample was then radiated while the internal temperature of the system was maintained using a circle of running water. Also, air with rate of 0.5 dm<sup>3</sup>/min was bubbled in the reaction solution continuously and meanwhile homogenized the suspension with continued stirring. A sampling of 2-mL solution was done at specific time intervals and filtered through a membrane filter (0.45 μm, Schleicher & Schuell, Germany). Finally, through its UV-vis absorption at 665 nm quantitative degradation of MB was determined. After the catalytic reaction, the photocatalyst was filtered, washed with water and ethanol, and dried. To ensure the efficacy of the catalyst, it was applied up to four cycles repeatedly and the results were recorded. For comparison, the MB photodegradation was done under the same conditions using TiO<sub>2</sub> P25 powder as photocatalyst. The efficiency of degradation was obtained using equation 1:

$$\text{Degradation efficiency (\%)} = C_0 - C / C_0 \times 100\% \quad (1)$$

where  $C_0$  is the absorbance of MB at 665 nm after the adsorption–desorption equilibrium and  $C$  is the absorbance of MB after regular irradiation.

## 2.5. Characterizations

Powder X-ray diffraction (XRD) patterns were provided with a Bruker-axs, D8 Advance model, using CuK $\alpha$  radiation ( $\lambda = 0.15406$  nm) between 20 °C and 80 °C by a step of 0.02. Fourier transform infrared (FT-IR) spectra were measured with a KBr pellet on a Shimadzu 4300 spectrometer. The morphology and particle size were investigated by the transmission electron microscopy (TEM) Leo 912 AB. The elemental analysis and purity of the products were determined by energy dispersive analysis of X-rays (EDX) on the same FE-SEM instrument. FE-SEM analyses were performed on MIRA 3 TESCAN-XMU (TESCAN, CZECH REPUBLIC). Diffuse reflectance UV–vis spectrum (DRS) conducted in the wavelength range of 200–800 nm using a spectrophotometer (Scinco S400, S. Korea). The samples specific surface area and pore properties were obtained using the Brunauer-Emmett-Teller (BET) and Barrett-Joyner-Halenda (BJH) models with nitrogen adsorption–desorption isotherms collected by Belsorp apparatus at 77 K. Electronic spectra (UV–vis) were taken by an Optizen 3220 UV–vis spectrophotometer.

## 3. Results and discussion

### 3.1. XRD analysis

The XRD patterns of TiO<sub>2</sub> P25 and dye-sensitized TiO<sub>2</sub> are shown in Figure 2. The diffraction peaks appearing in the XRD patterns show that the crystalline phase of the samples are a mix of crystal phase [7]. These peaks are in accordance with the typical diffraction peaks, No. 04-002-8296 and No. 04-003-0648. According to expectations, rutile phase peaks appeared very weak, and in the pattern it is not clear and is covered with the anatase phase peaks because only 14% of the TiO<sub>2</sub> P25 is formed by the rutile phase [35]. By comparing the two XRD patterns, it is noticeable that the

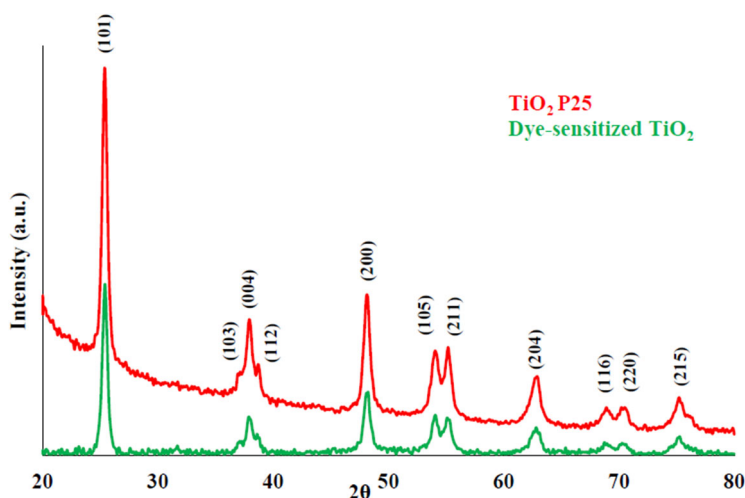


**Figure 2.** XRD pattern of TiO<sub>2</sub> P25 and dye-sensitized TiO<sub>2</sub>.

diffraction peaks of ruthenium complex is not assigned in dye-sensitized TiO<sub>2</sub>, which might be under the XRD limit [36]. From XRD patterns it can be concluded that the peak position and peak width of dye-sensitized TiO<sub>2</sub> remain unchanged compared to the bare TiO<sub>2</sub>, which reveals that the crystal structure and particle size of the TiO<sub>2</sub> catalyst remained unchanged and unaffected even by adsorption of ruthenium complex on the surface of TiO<sub>2</sub>. The nanocrystal size is calculated using Debye–Scherrer’s formula, from the [101] diffraction peak as the crystallite sizes is tabulated in Table 1.

### 3.2. FT-IR spectra

FT-IR spectra of unmodified TiO<sub>2</sub> powder and dye-sensitized TiO<sub>2</sub> are shown in Figure S1. Two strong absorption bands at 526 and 674 cm<sup>-1</sup> in the spectrum are assigned to the Ti-O vibrations in the unmodified TiO<sub>2</sub> powders and the band at about 3200 cm<sup>-1</sup> obviously relates to the vibration of Ti-OH [17, 37, 38]. As observed in the FT-IR spectrum of the ruthenium complex, the absorption bands at 1716 cm<sup>-1</sup> ν(C=O) and 1267 cm<sup>-1</sup> ν(C-O) refer to the carboxylic groups and confirm formation of the *cis/trans*-[Cl(L)Ru(*tpyz*)Ru(L)Cl](ClO<sub>4</sub>)<sub>2</sub> complex. According to previous literatures, the specific vibration bands of carboxylic acid groups appear in the regions 1705–1720 cm<sup>-1</sup> ν(C=O) and 1210–1320 cm<sup>-1</sup> ν(C-O) [39]. There are several absorption bands at 1653, 1429, 1392, and 1303 cm<sup>-1</sup> in the FT-IR spectrum of dye-sensitized TiO<sub>2</sub> which can be attributed to the asymmetric and symmetric stretching of –COO<sup>-</sup> [40]. The binding of the ruthenium complex to TiO<sub>2</sub> is confirmed by the disappearance of the C=O stretching band in the dye-sensitized TiO<sub>2</sub> spectrum [41].

### 3.3. FE-SEM, TEM, and SEM-EDX characterization

The morphological situation of TiO<sub>2</sub> P25 and dye-sensitized TiO<sub>2</sub> is analyzed by FE-SEM, TEM, and SEM-EDX. Figure 3(a–d) shows the FE-SEM and TEM of TiO<sub>2</sub> P25 and dye-sensitized TiO<sub>2</sub>. No obvious change was observed for the dye-sensitized TiO<sub>2</sub>

**Table 1.** Nanoparticle size, BET surface area and pore volume, mean pore diameter, nanocrystal size, band gap, and degradation%.

Samples	Mean pore diameter (nm)	BET surface area (m <sup>2</sup> /g)	Pore volume (cm <sup>3</sup> /g)	Nanocrystal size (nm)	Band gap (eV)	Degradation%
TiO <sub>2</sub> P25	13.56	86	0.2916	16.69	3.1	12.04
Dye-sensitized TiO <sub>2</sub>	16.07	91.80	0.3688	17.39	2.70	87

particles, and like TiO<sub>2</sub> particles, the sample is composed of spherical-like structures. Also, clumped or agglomerated ruthenium complex is not formed in observable size on the surface of the TiO<sub>2</sub> nano-powders and both samples have a lumpy structure. In order to confirm that the ruthenium complex is successfully distributed on the TiO<sub>2</sub> P25 surface, the samples are further characterized by EDX as shown in [Figure S2](#) and [Table 2](#). Although there is no bulky ruthenium complex on outside of TiO<sub>2</sub> nano-powder, SEM-EDX analyses confirm the presence of elements Ru, N, C and O on the surface of TiO<sub>2</sub> P25 nano-powder. Thus, the SEM-EDX can confirm the presence of ruthenium complex on the surface of TiO<sub>2</sub> P25. The grain diameter is around 17–22 nm that corresponds to the XRD results.

### 3.4. BET nitrogen adsorption–desorption isotherms

The special surface area is one of the important factors in photocatalytic reactions. The nitrogen adsorption and desorption isotherms are used to study the surface area and porosity of the photocatalyst. [Figure 4](#) shows the nitrogen adsorption and desorption isotherms, and the pore size distribution of samples is determined by the BJH method ([Figure S3](#)). According to the IUPAC classification, both TiO<sub>2</sub> P25 and dye-sensitized TiO<sub>2</sub> are mesoporous due to H3 hysteresis loop in the range of 0.2–1.0P/P<sub>0</sub>, which implies the existence of cylindrical-shape [42]. Some parameters are calculated from the N<sub>2</sub> isotherms such as the specific area, median pore diameters, and pore volume of the samples ([Table 1](#)). An increase in BET analysis of the surface area and the average pore size are in accordance with the obtained results of the XRD analysis which emphasizes the effective modifications of TiO<sub>2</sub> P25 sensitized by ruthenium complex.

### 3.5. Uv–vis adsorption spectra analysis

To investigate the influence of sensitizer on the light absorption and band gap of TiO<sub>2</sub>, the UV–vis absorption spectrum (DRS) and the Tauc-Mott (TM) plots, which are derived from the absorption spectra, can be used [43]. The following equation determines TM approximation for band gap energy:

$$(\alpha \times h\nu_{\text{photon}})^{1/r} = A(h\nu_{\text{photon}} - E_g) \quad (2)$$

where  $h$ ,  $\alpha$ ,  $\nu$ ,  $A$ , and  $E_g$  are the Planck constant, absorption coefficient, photon frequency, a constant, and band gap energy, respectively. The value of  $r$  is determined by the type of transfer which is 1/2 and 2 for direct and indirect, respectively. In a TM

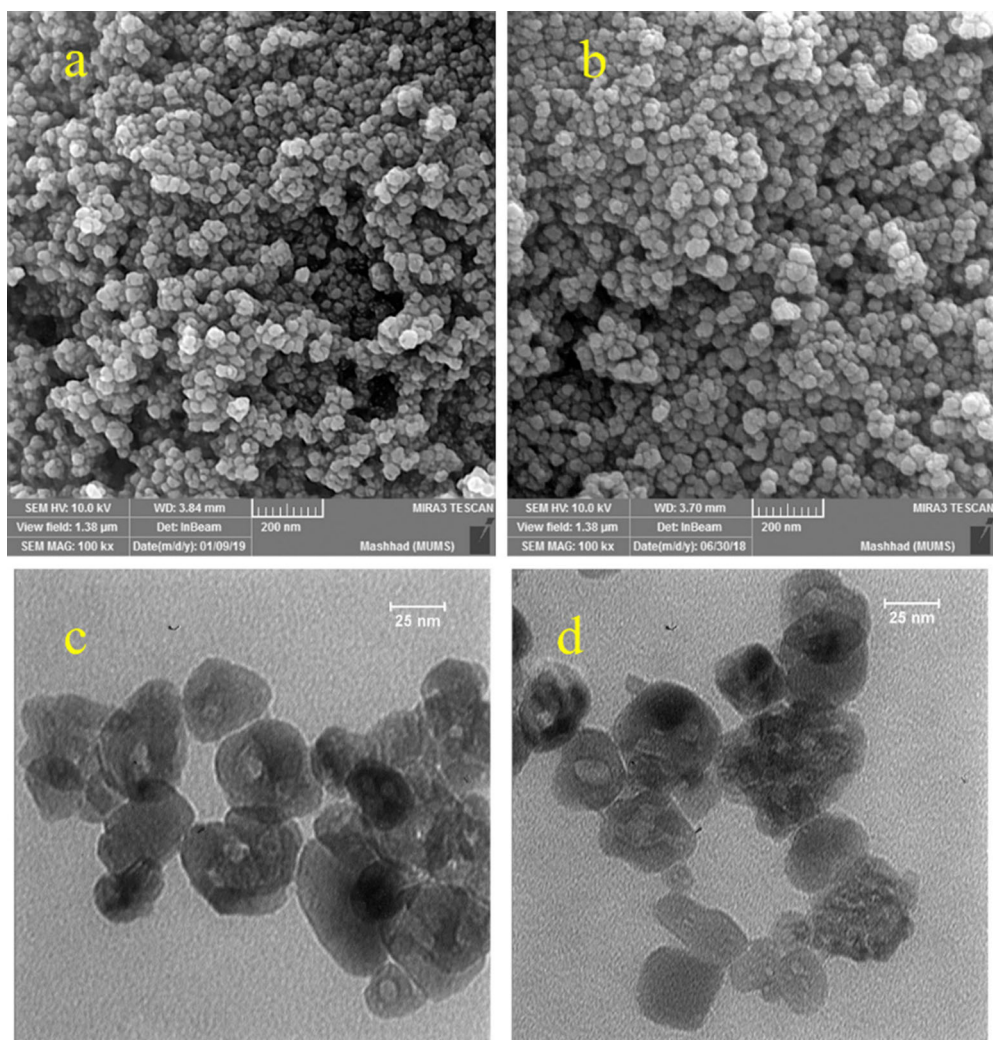


**Figure 3.** (a) SEM images of TiO<sub>2</sub> P25 and (b) dye-sensitized TiO<sub>2</sub>, and (c) TEM images of TiO<sub>2</sub> P25 and (d) dye-sensitized TiO<sub>2</sub>.

**Table 2.** Elemental analysis of samples.

Element	Weight% Samples	O%	Ti%	C%	N%	Ru%
TiO <sub>2</sub> P25		69.06	30.94	-	-	-
Dye-sensitized TiO <sub>2</sub>		55.34	17.13	9.07	17.88	0.58
The four cycle of dye-sensitized TiO <sub>2</sub>		54.33	17.73	10.18	17.38	0.38

plot,  $(\alpha \times h\nu_{\text{photon}})^{1/r}$  is plotted vs.  $h\nu_{\text{photon}}$  followed by extrapolation of the linear section of the plot to the  $h\nu_{\text{photon}}$  axis [44].

The UV-vis DRS spectra and plots of  $(\alpha h\nu)^2$  versus photon energy for TiO<sub>2</sub> P25 and dye-sensitized TiO<sub>2</sub> are displayed and compared in Figure 5. Through connection of the ruthenium complex to the TiO<sub>2</sub> surface, absorption and the intensity in the UV region is slightly red-shifted and increased, successively. It is seen that in the case of P25 the band gap obtained from  $(\alpha h\nu)^2$  versus energy plot is 3.12 eV. By connecting



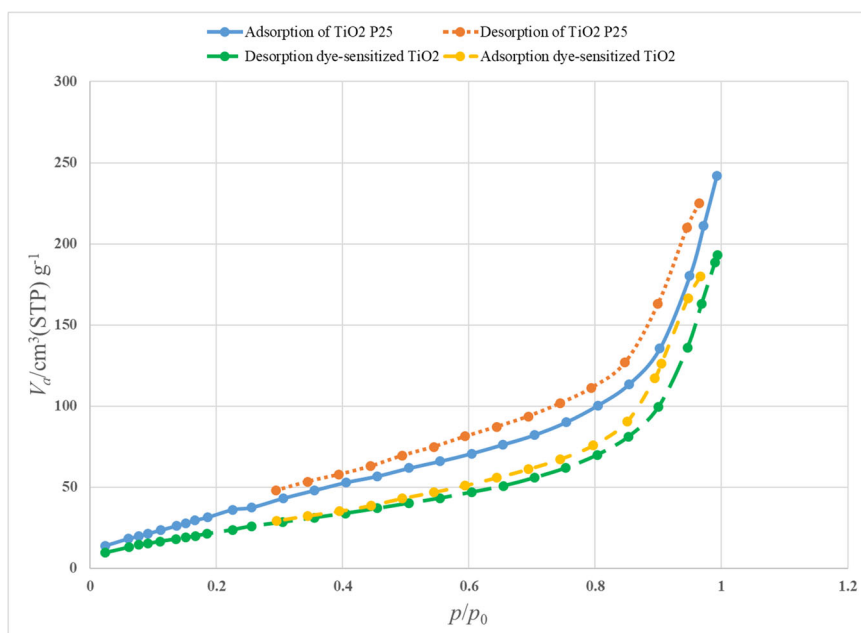


**Figure 4.** Nitrogen adsorption–desorption isotherm of  $\text{TiO}_2$  P25 and dye-sensitized  $\text{TiO}_2$ .

the dye to  $\text{TiO}_2$ , absorption edge significantly shifts to the visible light region, the absorption intensity in the visible region increases and the band gap for dye-sensitized  $\text{TiO}_2$  is calculated as 2.70 eV. No absorption band is seen above 400 nm for  $\text{TiO}_2$ , while dye-sensitized  $\text{TiO}_2$  shows visible light absorption from 400 to 800 nm.

UV-vis spectroelectrochemical experiments of the ruthenium complex were also measured by dissolving the ruthenium complex in DMF. Figure 6 shows the UV-vis spectra of the complex. The Ru complex showed strong transitions of  $\text{Ru}(d\pi)\text{-}tppz(\pi^*)$  at 565 nm and  $\text{Ru}(d\pi)\text{-}bpy(\pi^*)$  at 376 nm. The spin allowed ligand-centered (LC) ( $\pi\text{-}\pi^*$ ) (*tppz*) transitions create the intense absorption bands in the UV region [45].

### 3.6. Photocatalytic activity

The photocatalytic activities of  $\text{TiO}_2$  P25 and dye-sensitized  $\text{TiO}_2$  are evaluated by decreasing the absorption peak intensity to 665 nm in the “methylene blue” as an organic dye in aqueous solution under visible light irradiation ( $\lambda > 420$  nm). Figure 7 shows the change in the UV-vis spectrum of the MB aqueous solution in the presence of prepared photocatalyst. Degradation of MB versus the reaction time is investigated within three different situations: through photocatalyst with lack of light, visible light irradiation without the photocatalyst and in the presence of  $\text{TiO}_2$  P25 and dye-sensitized  $\text{TiO}_2$  with visible light irradiation. Figure S4 shows two trends, first the photocatalytic efficacy performed in the presence of photocatalyst without light, and second with visible light irradiation without the photocatalyst. These data reveal that the adsorption–desorption equilibrium of MB in the dark is fixed within 30 min and no significant degradation was observed under visible light in the absence of the photocatalyst after 2.7 h. Figure S4b shows the photocatalytic efficacy of  $\text{TiO}_2$  P25 and

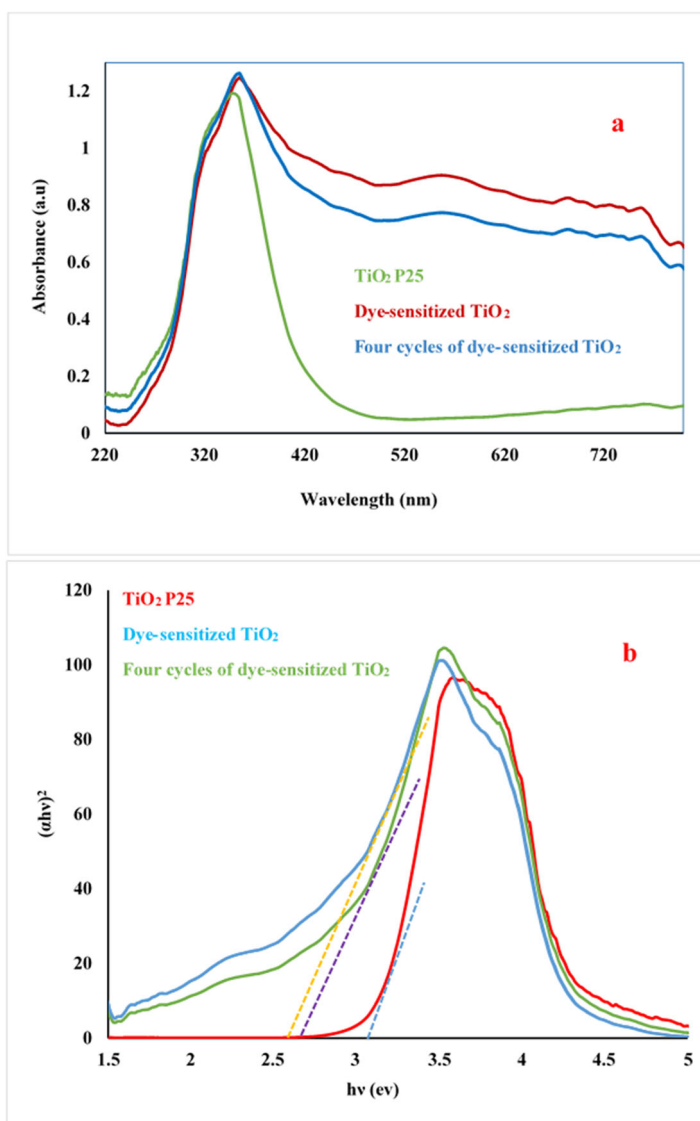


**Figure 5.** (a) UV-vis diffuse reflectance spectra of TiO<sub>2</sub> P25 and dye-sensitized TiO<sub>2</sub> and the fourth cycle of dye-sensitized TiO<sub>2</sub>; (b) corresponding TM plot of  $(\alpha h\nu)^2$  versus energy of the photon of TiO<sub>2</sub> P25 and dye-sensitized TiO<sub>2</sub> and the fourth cycle of dye-sensitized TiO<sub>2</sub>.

dye-sensitized TiO<sub>2</sub> with visible light irradiation, which reveals that TiO<sub>2</sub> P25 provides low photocatalytic activity under visible light and the degradation is only 12.04% in 2.4 h, while the dye-sensitized TiO<sub>2</sub> shows 87% degradation within the same time interval.

### 3.7. Photocatalytic kinetics

The photocatalytic degradation reactions mostly adopt the classical Langmuir-Hinshelwood kinetic model. In very low reactants concentration, the

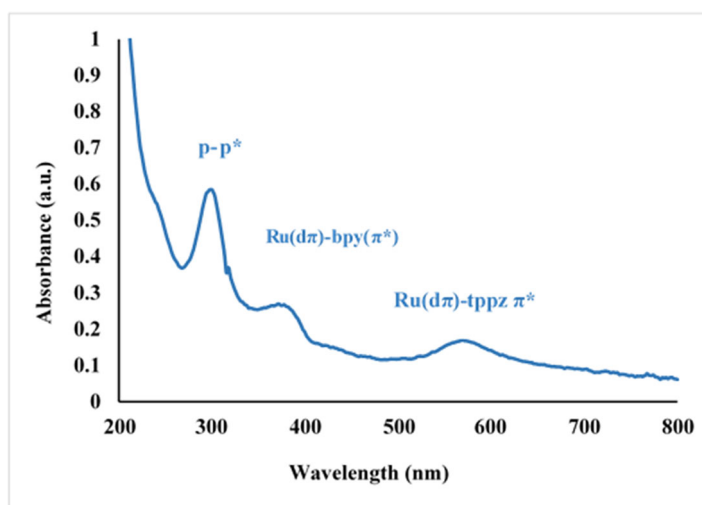


**Figure 6.** UV-vis spectroelectrochemical of *cis/trans*-[Cl(L)Ru(tppz)Ru(L)Cl](ClO<sub>4</sub>)<sub>2</sub>.

photocatalytic reaction can be simplified into a kinetic model [36]. A plot of  $-\ln(C/C_0)$  versus time displays a straight line:

$$-dc/dt = k_{ap} \times C = \ln(C_0/C) = k_{ap} \times t \quad (3)$$

where  $C_0$  is the initial concentration of MB,  $C$  is its concentration at time  $t$  and  $k_{ap}$  is the apparent first order rate constant (the slope of a plot of  $-\ln C/C_0$  versus time). The experimental results revealed that first order kinetic occurs in photocatalytic degradation of MB. The correlation coefficient values ( $R^2$ ) for  $-\ln C/C_0$  versus time are calculated to determine the photocatalytic degradation kinetics of MB on photocatalyst (Figure S5). It is clear that kinetic parameters verify the experimental ones.

### 3.8. Photocatalytic degradation mechanism

Photocatalytic degradation mechanism of TiO<sub>2</sub> P25 sensitized by ruthenium complex is discussed in the following aspects (Figure 8). First, the electrons are excited from the HOMO of the complex to the LUMO level with visible light irradiation (Equation 4). These electrons are transferred to O<sub>2</sub> molecules through inter system crossing (Equation 5). Also, the LUMO position of ruthenium complex as dye fits well with the energy requirements for efficient electron injection into CB of TiO<sub>2</sub>, so the excited charge can be injected from the excited state (LUMO) of dye into CB of TiO<sub>2</sub> (Equation 6). These electrons reduce oxygen molecules adsorbed on the titania particle and produced <sup>1</sup>O<sub>2</sub> to create superoxide radicals (O<sub>2</sub><sup>•-</sup>) (Equations 7 and 8) and reaction of O<sub>2</sub><sup>•-</sup> with the absorbed water on the semiconductor surface can generate hydroperoxyl (OOH<sup>•</sup>) radicals and then hydroxyl radicals (OH<sup>•</sup>) (Equations 9–11). In the photocatalytic process, the hydroxyl (HO<sup>•</sup>) and superoxide (O<sub>2</sub><sup>•-</sup>) radicals as the reactive oxidizing species (ROS) with the inorganic or organic pollutant including biological species (bacteria and virus) lead to the decomposition of pollutants by producing mineral salts of CO<sub>2</sub> and H<sub>2</sub>O (equations 12–15). Meanwhile, dye\* get the electrons from the solution to change into dye [36, 46–49].

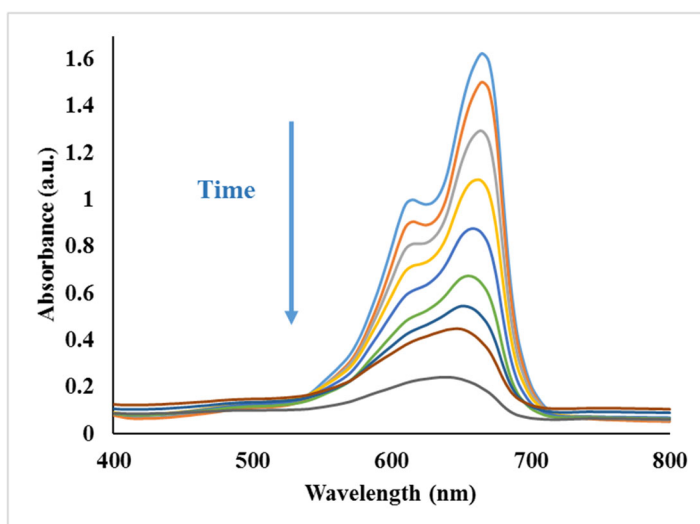
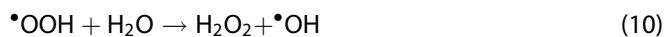
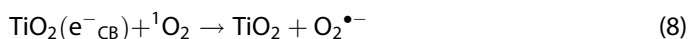
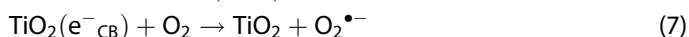


**Figure 7.** The change in the UV-vis spectrum of the MB aqueous solution in the presence of dye-sensitized TiO<sub>2</sub>.



### 3.9. Effect of photocatalysts recycling

The particular attention of industries to recycling of catalysts has increased attentions to the recyclability of photocatalysts. The catalyst recycling capability in the degradation of MB during 240-min cycles was experienced. For this purpose, after complete decomposition of MB, photocatalyst was recovered, then washed with water and ethanol, and dried. The degradation of MB was done under identical experimental conditions using dried sample again. The photocatalyst performance in four cycles is shown in Figure S6. In the first cycle, 87.02% MB is removed. After four cycles, gradual decrease in the degradation efficiency from 87.02% to 81.22% is observed. However, we can say there is no significant reduction in the photo degradation efficiency. It is confirmed that the coupled ruthenium complex on the TiO<sub>2</sub> surface exhibits good

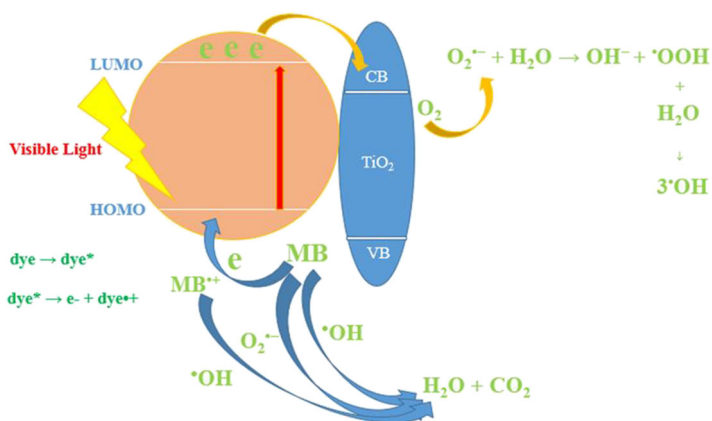


**Figure 8.** The photocatalytic mechanism diagram.

stability under irradiation. Therefore, the designed and synthesized structure in this project has a long-lasting effect and also a high recyclability. This gradual decrease and somehow deactivation of photocatalyst may be due to the fact that a small fraction of the anchored dye species was presumably disintegrated during the photocatalytic process or permanent adsorption of intermediates on the catalyst surface. We also analyzed the samples collected from the fourth cycle with DRS (Figure 5) and EDX (Figure S2), and the results confirmed that after four times the reaction was repeated, no changes were observed in the structure there. The UV-vis spectra show that after four times using the catalyst, it remains unchanged and the dye-TiO<sub>2</sub> binding is still strong and not affected by dissolution. Also, the results of EDX indicate that neither significant decomposition nor chemical modification of the dye-sensitized TiO<sub>2</sub> sensitizer takes place at the end of the photocatalytic process. Table S1 shows the comparison of the catalyst recycling capability of the prepared compound with other dye-sensitized TiO<sub>2</sub> compounds in the articles. The results of the table show that the catalyst recycling capability of the prepared compound is acceptable.

#### 4. Conclusion

*cis/trans*-[Cl(L)Ru(*tpz*)Ru(L)Cl](ClO<sub>4</sub>)<sub>2</sub> sensitized TiO<sub>2</sub> P25 is synthesized to improve the reaction toward visible light and dye-sensitized TiO<sub>2</sub>. The photocatalytic character was studied using different optical and microscopic techniques. Different results confirm the binding of ruthenium complex to titanium oxide nanoparticles. Accordingly, UV-vis adsorption spectra proved the photocatalyst is well absorbed in the visible region. The photocatalytic behavior of the synthesized photocatalyst was tested with MB photocatalytic degradation under visible light irradiation and showed superior degradation over TiO<sub>2</sub> P25. MB photocatalytic degradation adopted the first order kinetics reactions and the synthesized photocatalyst showed excellent recycling stability.

#### Disclosure statement

No potential conflict of interest was reported by the authors.

## Funding

This work was supported by the Ferdowsi University of Mashhad (3/46325).

## References

- [1] U.G. Akpan, B.H. Hameed. *J. Hazard Mater.*, 170, 520 (2009).
- [2] G. Qin, Z. Sun, Q. Wu, L. Lin, M. Liang, S. Xue. *J. Hazard Mater.*, 192, 599 (2011).
- [3] X. Yang, J. Qin, Y. Jiang, K. Chen, X. Yan, D. Zhang, R. Li, H. Tang. *Appl. Catal., B.*, 166–167, 231 (2015).
- [4] Q. Xiang, J. Yu, M. Jaroniec. *Chem. Soc. Rev.*, 41, 782 (2012).
- [5] J.-F. Huang, J.-M. Liu, P.-Y. Su, Y.-F. Chen, Y. Shen, L.-M. Xiao, D.-B. Kuang, C.-Y. Su. *Electrochim. Acta.*, 174, 494 (2015).
- [6] G. Varshney, S.R. Kanel, D.M. Kempisty, V. Varshney, A. Agrawal, E. Sahle-Demessie, R.S. Varma, M.N. Nadagouda. *Coord. Chem. Rev.*, 306, 43 (2016).
- [7] M. Wei, J. Wan, Z. Hu, Z. Peng, B. Wang. *Appl. Surf. Sci.*, 377, 149 (2016).
- [8] B. Cabir, M. Yurderi, N. Caner, M.S. Agirtas, M. Zahmakiran, M. Kaya. *Mater. Sci. Eng., B.*, 224, 9 (2017).
- [9] L.W. Zhang, H.B. Fu, Y.F. Zhu. *Adv. Funct. Mater.*, 18, 2180 (2008).
- [10] X.-L. Sui, Z.-B. Wang, M. Yang, L. Huo, D.-M. Gu, G.-P. Yin. *J. Power Sources*, 255, 43 (2014).
- [11] N. Yazdanpour, S. Sharifnia. *Sol. Energy Mater. Sol. Cells*, 118, 1 (2013).
- [12] C. Albay, M. Koç, İ. Altın, R. Bayrak, İ. Değirmencioglu, M. Sökmen. *J. Photochem. Photobiol., A*, 324, 117 (2016).
- [13] M. Rico-Santacruz, Á.E. Sepúlveda, C. Ezquerro, E. Serrano, E. Lalinde, J.R. Berenguer, J. García-Martínez. *Appl. Catal., B*, 200, 93 (2017).
- [14] B. O'regan, M. Grätzel. *Nature*, 353, 737 (1991).
- [15] T. Bessho, E. Yoneda, J.-H. Yum, M. Guglielmi, I. Tavernelli, H. Imai, U. Rothlisberger, M.K. Nazeeruddin, M. Grätzel. *J. Am. Chem. Soc.*, 131, 5930 (2009).
- [16] K.C.D. Robson, B.D. Koivisto, A. Yella, B. Spornova, M.K. Nazeeruddin, T. Baumgartner, M. Grätzel, C.P. Berlinguette. *Inorg. Chem.*, 50, 5494 (2011).
- [17] Y. Mahmiani, A.M. Sevim, A. Gül. *J. Photochem. Photobiol., A*, 321, 24 (2016).
- [18] M.K. Nazeeruddin, M. Grätzel. *Transition Metal Complexes for Photovoltaic and Light Emitting Applications*, Berlin Heidelberg: Springer-Verlag (2007).
- [19] G. Giuffrida, S. Campagna. *Coord. Chem. Rev.*, 135–136, 517 (1994).
- [20] D. Astruc. *Acc. Chem. Res.*, 30, 383 (1997).
- [21] K.D. Demadis, C.M. Hartshorn, T.J. Meyer. *Chem. Rev.*, 101, 2655 (2001).
- [22] B. Sarkar, R.H. Laye, B. Mondal, S. Chakraborty, R.L. Paul, J.C. Jeffery, V.G. Puranik, M.D. Ward, G.K. Lahiri. *J. Chem. Soc., Dalton Trans.*, 2097 (2002).
- [23] E.I. Solomon, T.C. Brunold, M.I. Davis, J.N. Kemsley, S.-K. Lee, N. Lehnert, F. Neese, A.J. Skulan, Y.-S. Yang, J. Zhou. *Chem. Rev.*, 100, 235 (2000).
- [24] F. Paul, C. Lapinte. *Coord. Chem. Rev.*, 178–180, 431 (1998).
- [25] B.S. Brunshwig, N. Sutin. *Coord. Chem. Rev.*, 187, 233 (1999).
- [26] D.P. Rillema, D.G. Taghdiri, D.S. Jones, L.A. Worl, T.J. Meyer, H.A. Levy, C.D. Keller. *Inorg. Chem.*, 26, 578 (1987).
- [27] M. Hunziker, A. Ludi. *J. Am. Chem. Soc.*, 99, 7370 (1977).
- [28] E.V. Dose, L.J. Wilson. *Inorg. Chem.*, 17, 2660 (1978).
- [29] R.R. Ruminiski, J.D. Petersen. *Inorg. Chem.*, 21, 3706 (1982).
- [30] J.D. Petersen, W. Murphy, Jr, R. Sahai, K. Brewer, R. Ruminiski. *Coord. Chem. Rev.*, 64, 261 (1985).
- [31] C.H. Braunstein, A.D. Baker, T.C. Streckas, H.D. Gafney. *Inorg. Chem.*, 23, 857 (1984).
- [32] R.R. Ruminiski, T. Cockroft, M. Shoup. *Inorg. Chem.*, 27, 4026 (1988).
- [33] N. Chanda, R.H. Laye, S. Chakraborty, R.L. Paul, J.C. Jeffery, M.D. Ward, G.K. Lahiri. *J. Chem. Soc., Dalton Trans.*, 3496, 3496 (2002).

- [34] C.M. Hartshorn, N. Daire, V. Tondreau, B. Loeb, T.J. Meyer, P.S. White. *Inorg. Chem.*, 38, 3200 (1999).
- [35] F. Gherardi, A. Colombo, S. Goidanich, R. Simonutti, L. Toniolo. In *Hydrophobe VII-7th International Conference on Water Repellent Treatment and Protective Surface Technology for Building Materials 205* (2014)
- [36] J. Niu, B. Yao, Y. Chen, C. Peng, X. Yu, J. Zhang, G. Bai. *Appl. Surf. Sci.*, 271, 39 (2013).
- [37] L. Luo, Y. Yang, A. Zhang, M. Wang, Y. Liu, L. Bian, F. Jiang, X. Pan. *Appl. Surf. Sci.*, 353, 469 (2015).
- [38] R. Rahimi, S. Zargari, A. Yousefi, M.Y. Berijani, A. Ghaffarinejad, A. Morsali. *Appl. Surf. Sci.*, 355, 1098 (2015).
- [39] J. Cui, J. Lu, X. Xu, K. Cao, Z. Wang, G. Alemu, H. Yuang, Y. Shen, J. Xu, Y. Cheng, M. Wang. *J. Phys. Chem. C.*, 118, 16433 (2014).
- [40] D. Chen, D. Yang, J. Geng, J. Zhu, Z. Jiang. *Appl. Surf. Sci.*, 255, 2879 (2008).
- [41] K.L. Materna, R.H. Crabtree, G.W. Brudvig. *Chem. Soc. Rev.*, 46, 6099 (2017).
- [42] R. Pierotti, J. Rouquerol. *Pure Appl. Chem.*, 57, 603 (1985).
- [43] J. Zhang, L. Zhang, X. Ma, Z. Ji. *Appl. Surf. Sci.*, 430, 424 (2018).
- [44] A.R. Amani-Ghadim, S. Alizadeh, F. Khodam, Z. Rezvani. *J. Mol. Catal. A: Chem.*, 408, 60 (2015).
- [45] V. Tondreau, A.M. Leiva, B. Loeb, D. Boys, L.K. Stultz, T.J. Meyer. *Polyhedron*, 15, 2035 (1996).
- [46] W. Choi, A. Termin, M.R. Hoffmann. *J. Phys. Chem.*, 98, 13669(1994).
- [47] A.J. Hoffman, E.R. Carraway, M.R. Hoffmann. *Environ. Sci. Technol.*, 28, 776 (1994).
- [48] C.A. Emilio, M.I. Litter, M. Kunst, M. Bouchard, C. Colbeau-Justin. *Langmuir*, 22, 3606 (2006).
- [49] V. Etacheri, C.D. Valentin, J. Schneider, D. Bahnemann, S.C. Pillai. *J. Photochem. Photobiol., C*, 25, 1 (2015).